frontiers in Materials

ORIGINAL RESEARCH
published: 25 August 2020
doi: 10.3389/fmats.2020.00234

Bismuth Sulfide Nanorods as Efficient Photothermal Theragnosis Agents for Cancer Treatment

*Jing Jiang†, Xin Che†, Yiwen Qian, Luoziyi Wang, Yu Zhang and Zhiliang Wang**

Department of Ophthalmology, Huashan Hospital, Fudan University, Shanghai, China

Bi_2S_3 nanostructures can theoretically have photothermal properties. However, there are few reports on the application of bismuth sulfide in photothermal therapy due to the poor photothermal effect. To address this problem, herein we obtained Bi_2S_3 nanorods with defect structures via a facile method. Due to the special shape and defects, the Bi_2S_3 nanorods exhibited a strong absorption band in the NIR region, thus showed excellent photothermal effect. The photothermal conversion efficiency of Bi_2S_3 nanorods was calculated to be as high as 78.1% due to the strong NIR absorption. Importantly, the photothermal ablation experiments both *in vitro* and *in vivo* proved that the Bi_2S_3 nanorods can effectively kill cancer cells under the irradiation of an 808 nm laser. In addition, Bi_2S_3 nanorods can be used as effective CT imaging agents due to inherently high X-ray attenuation coefficient of bismuth. Our work demonstrated that the Bi_2S_3 nanorods were very promising photothermal nanoplatforms for photothermal therapy of cancers, guided by CT imaging.

Keywords: Bi_2S_3 nanorods, photothermal agents, CT imaging, photothermal therapy, photothermal conversion efficiency

OPEN ACCESS

Edited by:
Guanjie He,
University of Lincoln, United Kingdom

Reviewed by:
Nuo Yu,
Donghua University, China
Jichun Liu,
908th Hospital of the PLA, China

***Correspondence:**
Zhiliang Wang
ophwzl@163.com

†These authors have contributed equally to this work

Specialty section:
This article was submitted to Biomaterials, a section of the journal Frontiers in Materials

Received: *20 May 2020*
Accepted: *25 June 2020*
Published: *25 August 2020*

Citation:
Jiang J, Che X, Qian Y, Wang L, Zhang Y and Wang Z (2020) Bismuth Sulfide Nanorods as Efficient Photothermal Theragnosis Agents for Cancer Treatment. Front. Mater. 7:234. doi: 10.3389/fmats.2020.00234

INTRODUCTION

Photothermal therapy (PTT), which utilizes photothermal agents to convert near-infrared (NIR, 700–1400 nm) light energy into heat energy to "cook" cancer cells, has attracted increasing attention in recent years (Li et al., 2018). Some progresses have been achieved in the research of photothermal agents, but the application of photothermal therapy still faces considerable challenges (Yang et al., 2019). What's more, only a few of the nanostructured materials obtained by chemical synthesis that have been reported so far exhibit the absorption properties necessary for near-infrared light-to-heat conversion materials. Gold nanostructures have been extensively studied at the initial development stage of photothermal agents (Poper et al., 2007; Wang et al., 2009; Liu et al., 2012). Due to their adjustable absorption bands from the visible region to the near-infrared region, the gold nanostructures possess attracting photothermal performances. However, these gold nanostructures, especially gold nanorods, irreversibly transform into nanoparticles under the irradiation of NIR lasers (Tian et al., 2013). Therefore, several kinds of photothermal agents (including graphene oxides, semiconductors, and organic materials) were developed as alternatives to gold nanostructures (Chen et al., 2013). However, most of reported photothermal agents are hydrophobic, so complex hydrophilic modification processes are needed to make them meet the requirements of photothermal therapy applications (Hessel et al., 2011; Tian et al., 2011; Li et al., 2014). Since the hydrophilic modification will change the dielectric constant of the nanostructure,

the optical absorption properties of the nano-agents would be affected (Hessel et al., 2011). In addition, the 808 nm wavelength is widely used to study the photothermal effect of photothermal agents. The safely limit power density of the 808 nm laser on the skin is too low (∼0.33 W cm^{-2}) (Robinson et al., 2010). At this power density, the photothermal effects produced by photothermal agents are mostly difficult to kill cancer cells due to the poor photothermal performance of photothermal nano-agents (Liu et al., 2016; Zhang et al., 2016). Most of the photothermal agents reported so far have a single function and do not have imaging capabilities (Chang et al., 2013; Li et al., 2014). In this way, the early development of cancer cannot be monitored, which delays the timing of cancer treatment. There are also some reported photothermal agents that can simultaneously perform photothermal treatment and imaging diagnosis of tumors, but there are also certain problems. For example, Cu_3BiS_3 has photothermal effect and CT imaging capability, but the photothermal efficiency is low (Li et al., 2015). Therefore, in order to meet the severe requirements of photothermal therapy in the future, it is of great necessity to explore novel photothermal agents with excellent photothermal effect and multifunction.

It has been reported that Bi_2S_3 nanostructures with a direct band gap structure can exhibit a local plasma resonance effect (LSPR) in NIR region (Song et al., 2015). Moreover, due to its excellent biocompatibility and properties with photothermal effect resulted from intrinsic band gap absorption; Bi_2S_3 nanostructures have proved to be a promising photothermal agent (Xie et al., 2017). Additionally, bismuth is a high atomic number element with a relatively high X-ray attenuation coefficient, which can be used for CT imaging detection to observe the development of early tumors in cancer (Ai et al., 2011). However, because the absorption of bismuth sulfide is derived from the intrinsic band gap, it is difficult to adjust its optical properties, and it also makes its absorption coefficient and photothermal efficiency low. Therefore, there are few reports on the application of bismuth sulfide in photothermal therapy. Previous studies have confirmed that nano-agents can have absorption bands in the near infrared region due to their special morphology (Chen et al., 2010; Xu et al., 2012; Li W. et al., 2013). For example, gold nanorods may have long-axis absorption peaks in the near infrared region compared to gold nanoparticles (Chen et al., 2010). Thus bismuth sulfide with special morphology may have an absorption peak in the near infrared region. In general, Bi_2S_3 nanostructures can theoretically have excellent photothermal properties and CT imaging capabilities.

In this work, Bi_2S_3 nanorods served as photothermal theragnosis agents were prepared via a facile method. Due to the special shape and defects, the Bi_2S_3 nanorods exhibited a strong absorption band in the NIR region, thus showed excellent photothermal effect with a photothermal conversion efficiency up to 78.1%. Importantly, Bi_2S_3 nanorods can effectively kill cancer cells both *in vitro* and *in vivo* under the irradiation of an 808 nm laser. In addition, Bi_2S_3 nanorods can be used as effective CT imaging agents due to inherently high X-ray attenuation coefficient of bismuth. Our work demonstrated that the Bi_2S_3 nanorods are promising photothermal nanoplatforms for photothermal therapy of cancers, guided by CT imaging.

MATERIALS AND METHODS

Synthesis of Bi_2S_3 Nanorods

Bi_2S_3 nanorods were synthesized by a modified solvothermal method. Under magnetic stirring, 1 mmol of $Bi(NO_3)_3$ and 1.5 mmol of sodium diethyldithiocarbamate were fully dissolved in ethylene glycol (EG, 25 mL) and polyethylene glycol (PEG, M_W = 400 Da, 15 mL). The solution was then transferred to a 50 mL stainless steel reactor and kept at 180°C for 24 h. The black products can be obtained by ethanol washing and centrifugation.

Characterization

The morphology, microstructure, and size of the Bi_2S_3 nanorods can be determined by TEM. The XRD test was performed using a Bruker D4 X-ray diffractometer using Cu Ka radiation (λ = 0.15418 nm). The XPS test was performed on X-ray photoelectron spectrometer. The UV-vis-NIR absorption spectrum data was obtained from Shimadzu's UV-vis spectrophotometer. The released ions can be determined by Leeman laboratory inductively coupled plasma atomic emission spectrometer.

In order to measure the photothermal conversion performance of Bi_2S_3 nanorods, the light source was an 808 nm wavelength semiconductor laser with adjustable external power (0–1 W). 0.1 mL of nanorod dispersion with different concentrations was irradiated by an 808 nm laser. The output power was independently calibrated by a portable optical power meter and is ∼0.2 W, with a spot size of ∼0.66 cm^2. The temperature was recorded every 5 s by a thermal imaging camera.

To further evaluate the photothermal performance of Bi_2S_3 nanorods, we tested the photothermal efficiency of 40 ppm nanorods using a previous reported method (Roper et al., 2007). The Bi_2S_3 nanorods were dispersed in deionized water and continuously irradiated by an 808 nm laser (0.3 W cm^{-2}). The radiation source was immediately turned off when a steady-state temperature rise was achieved, and the temperature decrease was recorded to test the heat transfer rate of the system. The calculation formula (1) of the photothermal conversion efficiency (η_T) is as follows:

$$\eta_T = \frac{\mathrm{hA}(\mathrm{T_{max}} \mathrm{T}_{amb}) - Q_0}{I(1 - 10^{-A_\lambda})} \tag{1}$$

In which I is the laser power, A_λ is the absorption at the excitation wavelength. A is the surface area of the container. h is the heat transfer coefficient. T_{max} is the highest temperature of the system, and T_{amb} is the room temperature. Q_0 is the heat input rate (mW). The value of hA is obtained by the following formula (2):

$$\tau_s = \frac{m_D C_D}{hA} \tag{2}$$

Among them, τ_s is the time constant of sampling system. m_D and C_D are the mass (0.1 g) and specific heat capacity (4.2 J/g) of the

dispersed nanoparticle media, respectively. The value of τ_s can be obtained by formula (3):

$$t = -\tau_s \ln\theta = -\tau_s \ln\left(\frac{T - T_{amb}}{T_{\max} - T_{amb}}\right) \quad (3)$$

Therefore, the time constant of the system heat transfer can be obtained by the linear relationship between the cooling time and the negative natural logarithm of the temperature driving force.

CT Imaging

Bi_2S_3 nanorods aqueous dispersion (100 μL) with varied concentrations was placed in PE tubes; these PE tubes were fixed with a self-made device, and directly used a micro-CT imaging system.

EL-4 tumor (∼5 × 8 mm) model mice were first anesthetized with 100 μL 10% trichloroacetaldehyde, intratumoral injection of nanostructured PBS dispersion (100 μL, 5 mg mL-1), and the mice were scanned via micro-CT imaging system before and after the injection of nanorods. Scanning parameters are consistent with those of *in vitro* experiments. CT images were reconstructed on the same workstation using software provided by the supplier. The CT value was obtained by the software of CT imaging workstation. All animal experiments are conducted according to the guidelines of the Institutional Animal Care and Use Committee of the Huashan Hospital affiliated to Fudan University.

Photothermal Treatment of Cancer Cells *in vitro*

EL-4 cells are distributed in 96-well plates at a density of 10,000 per well. The cells were incubated in an RPMI-1640 medium at a temperature of 37°C and a CO_2 concentration of 5%. Subsequently, the cells were washed with PBS three times. 100 μL of Bi_2S_3 nanorods dispersed in PBS at different concentrations was then added to the wells, and the incubation was continued for 24 h. An 808 nm laser with a power density of 0.3 W cm^{-2} (power: ∼0.2 W, spot size: ∼0.66 cm^2) was used to irradiate the cells for 5 min. Cell survival rate can be determined by CCK-8 essay. In order to optimize the effect of laser power density on cell viability, 100 μL of Bi_2S_3 nanorod dispersion with a concentration of 40 ppm was added to the wells, and the incubation was continued for 24 h. An 808 nm laser with varied power density was used to irradiate the cells for 5 min. Then CCK-8 evaluation was used to measure the cell viability. All tests are performed independently three times.

Photothermal Therapy of Cancer Cells *in vivo*

The mice were inoculated with 1.5 × 10^6 EL-4 cells. When the tumor diameter of the mice grew to 5–8 mm for 3 weeks, the mice were divided into four groups (5 mice in each group) randomly. Group 1: intratumoral injection of Bi_2S_3 nanorods (i.e., NRs); Group 2: intratumoral injection of normal saline and irradiation with 808 nm laser (i.e., NIR); Group 3: intratumoral injection of Bi_2S_3 nanorods and irradiation with 808 nm laser with a power density of 0.3 W cm^{-2} (i.e., 0.3Treatment); Group 4: intratumoral injection of Bi_2S_3 nanorods and irradiation with 808 nm laser with a power density of 0.5 W cm^{-2} (i.e., 0.5Treatment). For Group 1 and 2, the potential *in vivo* toxicity of Bi_2S_3 nanorods or NIR laser alone was mainly investigated. For group 3 and 4, the two groups were examined for the effect of power density on cancer cells under the combined action of Bi_2S_3 nanorods and 808 nm lasers. For groups 2 and 4, they were investigated to evaluate the photothermal effect *in vivo* of Bi_2S_3 nanorods. After different treatments, tumor volume and body weight of the mice are measured every 2 days. Then the mice were sacrificed and the tumors were removed from the mice and embedded in paraffin to make 4 μm slices. These slices were stained with H&E, then inspected with the fluorescent lens of the Zeiss lens, and the image was processed with the Zeiss image camera system.

Biocompatibility Evaluation *in vivo*

Healthy mice were intravenously injected with 10 mg·kg^{-1} of the Bi_2S_3 nanorods. Major organs, including lung, liver, spleen, kidney and heart, were achieved at different time points (i.e., 1, 7, 14, 21 days, n = 3). These organs were then solubilized, and determined by ICP-AES analysis to confirm the content of bismuth. Blood samples from the Bi_2S_3 nanorod group and PBS group were collected at the different time points (i.e., 0, 1, 7, 14, 21 days) to evaluate the aspartate aminotransferase (AST) and alanine aminotransferase (ALT). In addition, the major organs were collected for histological analysis pre- and post-injection of Bi_2S_3 nanorods at varied time points (i.e., 7, 14, 21 days).

RESULTS AND DISCUSSION

In order to prepare Bi_2S_3 nanorods (NRs), $Bi(NO_3)_3$, Sodium diethyldithiocarbamate and polyethylene glycol (PEG) were fully dissolved in ethylene glycol (EG) to form a uniform solution, which was then transferred to a reaction kettle and reacted at 180^{o}C for 24 h. Black products can be obtained after centrifuge and washing with water for three times. In order to clarify the crystal phase of the synthesized products, we characterized the sample with an X-ray diffractometer. All the main peaks of X-ray diffraction patterns (**Figure 1a**) of the products can be well matched with the peaks of orthorhombic structured Bi_2S_3 (JCPDS No. 17-0325). From **Figure 1a**, the very narrow and intense peak of (130) indicated that the nanostructure grew along the (130) direction. Subsequently, we analyzed the elemental composition and oxidation states of the products, as shown in **Figure 1b**. The X-ray photoelectron spectrum (XPS) revealed that the sample contained five elements, i.e., Bi, S, O, N, and C. The elements O, N, and C were from the reaction precursors, indicating that the sample contained only Bi and S. The high resolution XPS of Bi and S indicated that the valence of bismuth was trivalent, and the valence of sulfur was a mixture of monovalent and divalent, meaning that there existed defect structure in Bi_2S_3 (**Supplementary Figure S1**). The TEM image (**Figure 1c**) revealed that the Bi_2S_3 nanostructures were monodispersed nanorods with sizes ranging from 50 to 300 nm. From the

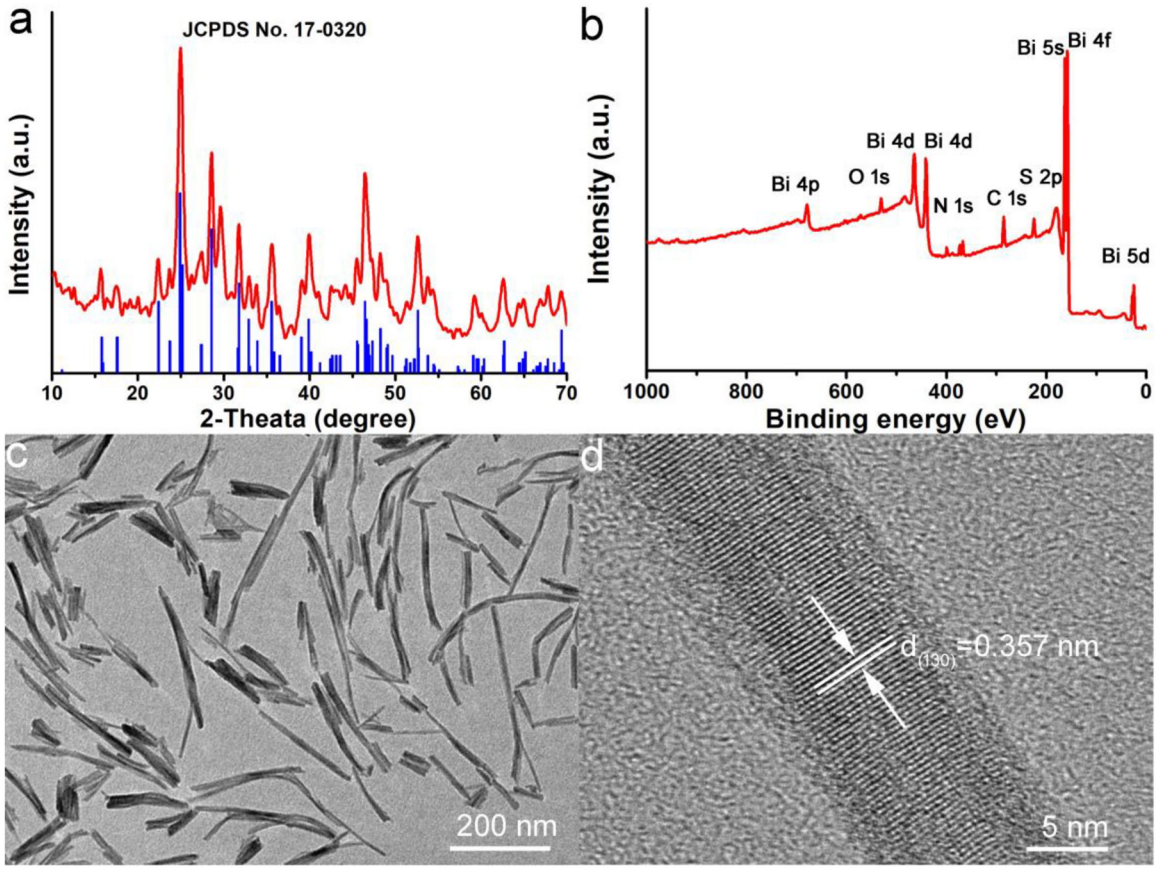

FIGURE 1 | (a) XRD pattern of Bi_2S_3 nanorods. **(b)** XPS spectra of Bi_2S_3 nanorods. **(c)** TEM and **(d)** high resolution TEM of Bi_2S_3 nanorods.

high resolution TEM image (**Figure 1d**), it can be seen that these nanorods were formed by the directional arrangement of bundled 5–22 nm nanorods. The microstructure information of nanorods can be further obtained from high-resolution TEM. The interplanar spacing was 0.357 nm, corresponding to the spacing of the (310) plane of the orthorhombic structured Bi_2S_3. Therefore, it can be concluded that Bi_2S_3 nanorods were successfully prepared.

Since the surface ligand of Bi_2S_3 nanorods was PEG, the nanorods were hydrophilic and can be directly dispersed in water without complicated surface modification. The absorption property of Bi_2S_3 nanorods in the NIR region has an important influence on its photothermal effect. **Figure 2A** shows the UV-vis absorption spectrum of Bi_2S_3 nanorod aqueous dispersions. Surprisingly, there was a broad and strong absorption band in the NIR region which was very different from those of Bi_2S_3 nanomaterials. After the concentration of the nanorod aqueous dispersion was determined by inductively coupled plasma atomic emission spectrometer (ICP-AES), the excitation coefficient of Bi_2S_3 nanorods can be calculated to be 12.3 L g^{-1} cm^{-1} which was higher than those of previously reported Bi_2S_3 nanomaterials (Song et al., 2015; Xie et al., 2017). The strong NIR absorption motivated us to evaluate their photothermal effect of Bi_2S_3 nanorods. Although the maximum absorption wavelength of Bi_2S_3 nanorods was centered at 550 nm (**Figure 2A**), 550 nm is located in the visible light region which exhibits weak penetration and strong scattering in biological tissue. The wavelength of the light source that excites the photothermal agent is in the range of 600–1400 nm. According to the optical properties of Bi_2S_3 nanorods, 808 nm lasers were chosen to study the photothermal effect. We measured the temperature change of the nanorods with a concentration gradient under the irradiation of an 808 nm laser. As shown in **Figure 2B**, the temperature of Bi_2S_3 nanorod dispersion at a concentration of 40 ppm increased by 22^{o}C under an 808 nm laser irradiation at a power density of 0.3 W cm^{-2}, while the temperature of pure water only increased by less than 2^{o}C at the same conditions. It can be concluded that Bi_2S_3 nanorods can quickly and efficiently convert 808 nm laser energy into heat energy. Thus the Bi_2S_3 nanorods showed excellent photothermal effect. Photothermal stability is an important indicator for evaluating photothermal agents. As shown in **Figure 2C**, the maximum temperature rise showed almost no changes after five circles of laser on/off, indicating the excellent photothermal stability of Bi_2S_3 nanorods. We also measured the optical properties of Bi_2S_3 nanorods after the four circles of laser ON/OFF. The absorption intensity showed little

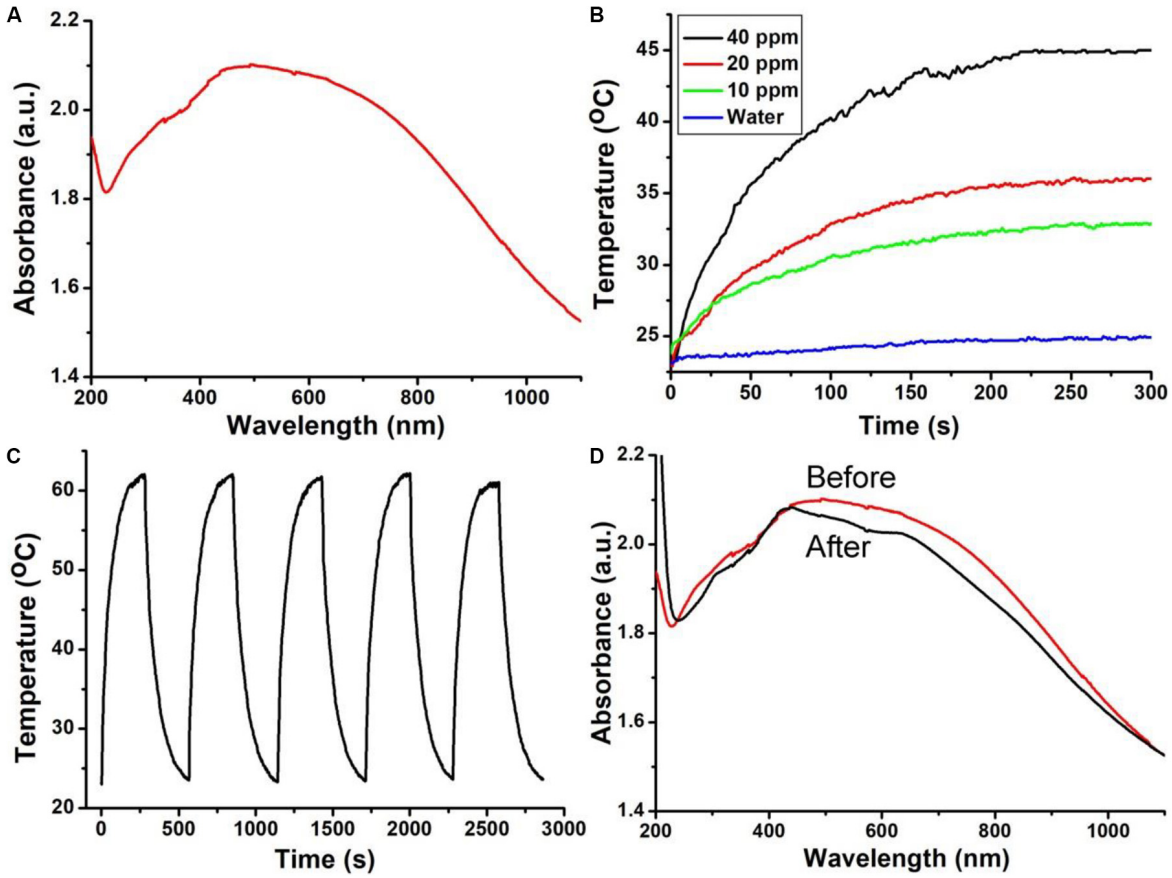

FIGURE 2 | (A) UV-vis spectra and **(B)** photothermal effect of Bi_2S_3 nanorods. **(C)** Temperature change of Bi_2S_3 nanorods during the five circles of laser ON/OFF. **(D)** UV-vis spectra of Bi_2S_3 nanorods before (red line) and after photothermal stability measurement.

decrease (**Figure 2D**), further confirming the good photothermal stability. Therefore, Bi_2S_3 nanorods can be very promising photothermal agents due to the excellent photothermal effect and photothermal stability.

In order to further study the photothermal properties of Bi_2S_3 nanorods, we calculated the photothermal conversion efficiency of the Bi_2S_3 nanorods using a method similar to the previous report (Roper et al., 2007). We recorded the temperature change of the nanorod solution (40 ppm) under the irradiation of an 808 nm laser (0.25 W) with time until an equilibrium temperature was reached (**Figure 3A**). The time constant (τ_s) of the system heat transfer can be obtained from **Figure 3B**, and was calculated to be 63.9 s. Based on the data in **Figures 2A**, **3**, we calculated the photothermal conversion efficiency of the Bi_2S_3 nanorods driven at 808 nm to be 78.1% which was much higher than some previously reported semiconductor pohotothermal agents (Song et al., 2015). The as-prepared Bi_2S_3 nanomaterials exhibited higher excitation coefficient (12.3 L g^{-1} cm^{-1}) than those of previously reported Bi_2S_3 nanomaterials (Song et al., 2015; Xie et al., 2017). Usually, the NIR absorption of Bi_2S_3 nanomaterials is derived from intrinsic band gap which resulted in low excitation coefficient. In our work, the Bi_2S_3 nanomaterials possessed defect structure and special shape. The defect structure made the Bi_2S_3 nanomaterials have metal-like absorption properties. Meanwhile, the special shape made its absorption peak blue shift (Chen et al., 2010). Therefore, the as-prepared Bi_2S_3 nanomaterials showed higher excitation coefficient due to the defect structure and special shape, contributing to the high photothermal conversion efficiency. Similar to the $Cu_{2-x}Te$ nanocrystals, the optical property of these Bi_2S_3 nanorods can be adjusted through the shape and defects (Li W. et al., 2013). Therefore, the Bi_2S_3 nanorods can be expected to be used as photothermal agents for cancer treatment by 808 nm laser-driven photothermal therapy.

The excellent photothermal properties of Bi_2S_3 nanorods inspired us to study the therapeutic effects of the nanorods on tumor cells. Prior to this, we evaluated the toxicity of the Bi_2S_3 nanorods. Bi_2S_3 nanorods incubated with EL-4 cancer cells for 24 h, and then a standard CCK-8 essay was used to evaluate the cell survival rate. It was found that the cell viability was 92% when the concentration was 40 ppm (**Supplementary Figure S2A**) at which the temperature of Bi_2S_3 nanorods dispersion could reach 22°C and was enough to kill cancer cells. When the concentration reached up to 160 ppm, the cell survival rate was still as high as 85%, indicating that Bi_2S_3 nanorods showed low toxicity. Previously reported photothermal agents used a larger laser power for photothermal treatment due to the low photothermal

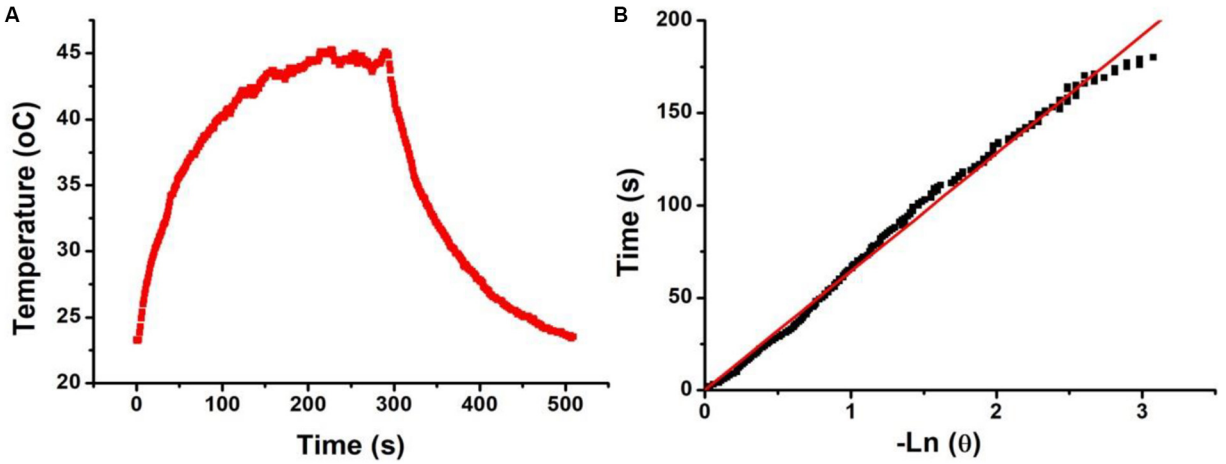

FIGURE 3 | (A) Temperature change of Bi_2S_3 nanorods (40 ppm) irradiated by an 808 laser for 300s, then shut off the laser for 300 s. **(B)** Time constant of Bi_2S_3 nanorods, τ_s = 63.9.

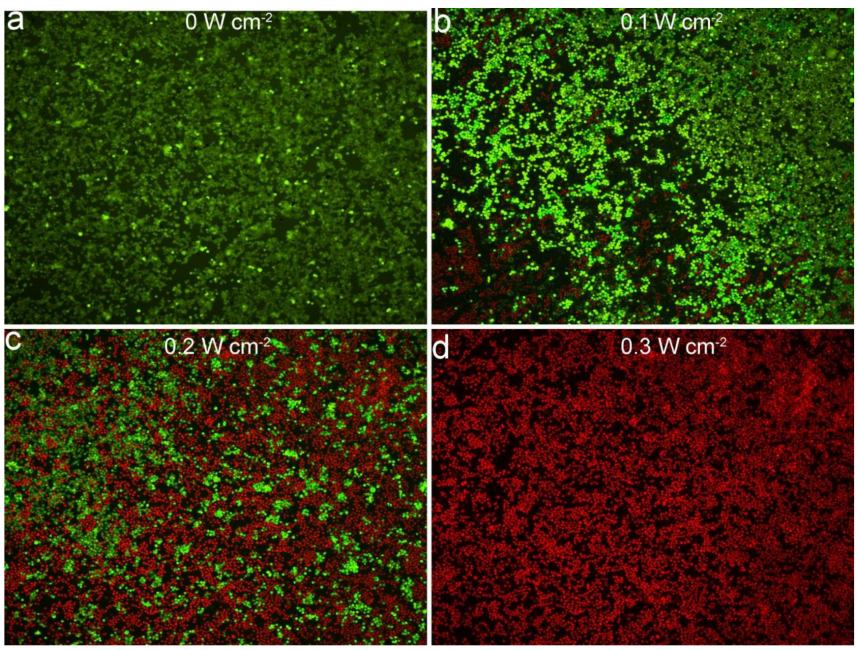

FIGURE 4 | Images of staining live/dead cells treated with an 808 nm laser at different power density. **(a)** 0 W cm^{-2}. **(b)** 0.1 W cm^{-2}. **(c)** 0.2 W cm^{-2}. **(d)** 0.3 W cm^{-2}. Magnification: 100 times.

efficiency of photothermal agents. We then studied the effect of photothermal treatment of the nanorods (40 ppm) on cancer cells under different laser power density conditions. As shown in **Supplementary Figure S2B**, cell viability decreased as the laser power density increased. When the laser power density was 0.3 W cm^{-2}, the cell viability is less than 2%, indicating an excellent phototherapy of cancer cells *in vitro*. In order to observe vividly the effect of the photothermal effect of Bi_2S_3 nanorods on the El-4 cells, we stained the live and dead cells with calcein-AM and propidium iodide. **Figure 4** shows the confocal micrographs of the cells after photothermal treatment under an 808 nm laser with indicated power density. It indicated that the dead cells increased more with the increase of power density, and the results of live/dead cell staining analysis were matched well with CCK-8 assay in **Supplementary Figure S2B**. Both the CCK8 assay and the live/dead cell staining analysis confirmed that Bi_2S_3 nanorods combined with NIR laser irradiation showed a good phototherapy effect on El-4 cell proliferation.

CT imaging is an effective detection tool which is widely used in clinical diagnosis and medical research. Many elements with high X-ray attenuation coefficients have been developed to be used as CT imaging diagnostic agents, including bismuth,

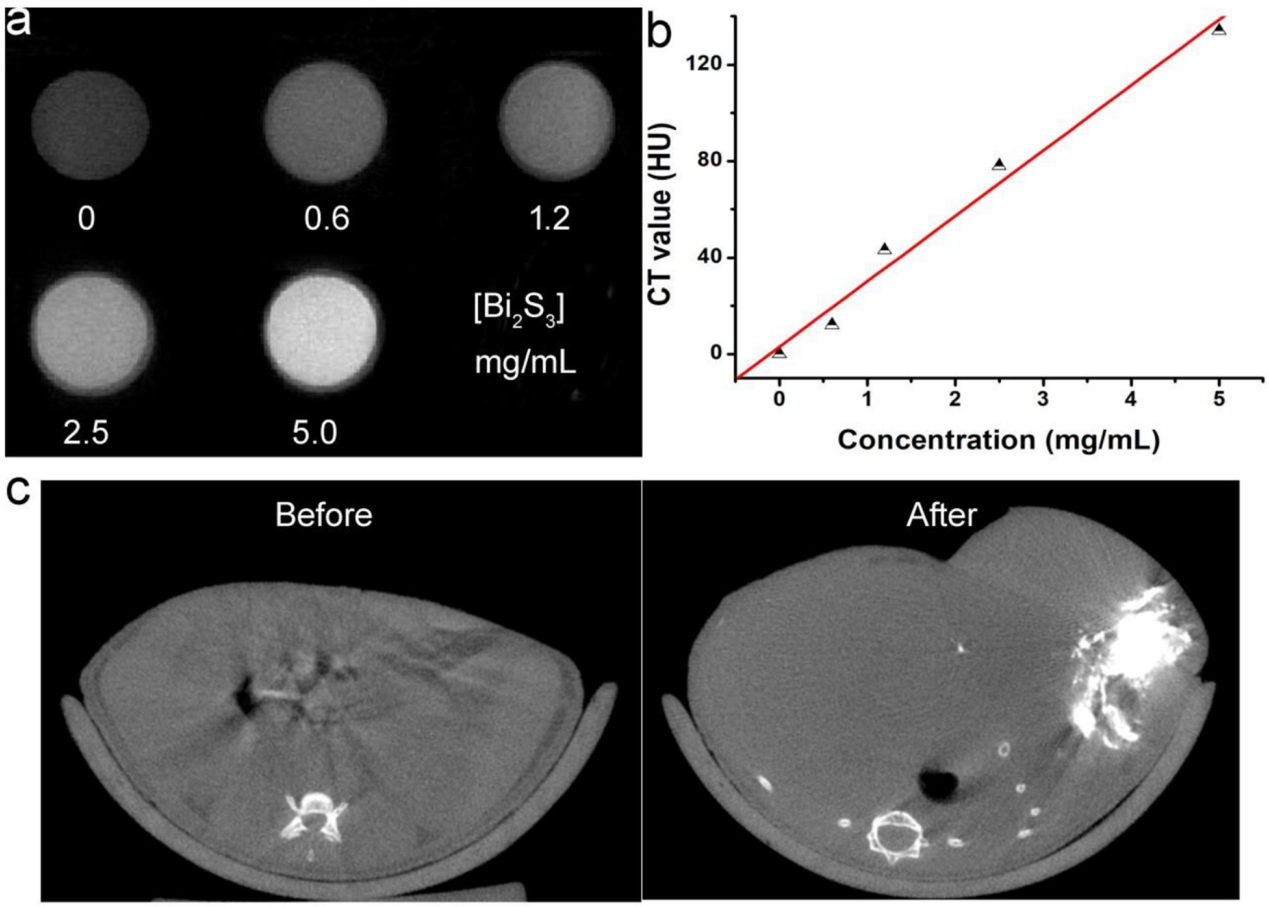

FIGURE 5 | (a) CT signals of Bi_2S_3 nanorods. **(b)** CT value as a function of the concentration of Bi_2S_3 nanorods. **(c)** CT image of a mouse before (left) and after (right) the injection of Bi_2S_3 nanorods.

iodine, gold, lanthanides, etc. Thus Bi_2S_3 nanorods can be used for CT imaging detection. We placed Bi_2S_3 nanorods aqueous dispersions with different concentrations in test tubes for CT imaging experiments. **Figure 5a** shows CT images of Bi_2S_3 nanorods aqueous dispersions with different concentrations. It was obviously observed that the CT signal intensity gradually increased as the concentration increased. At the same time, it can be seen in **Figure 5b** that the HU value of the Bi_2S_3 nanorods increased linearly with the concentration, and the slope (**Figure 5b**) of the HU value of the Bi_2S_3 nanorods was about 27.1 HU L/g, which was higher than those of some other nanomaterial (Li J. et al., 2013; Li et al., 2015). Subsequently, we used EL-4 tumor model mice to evaluate the *in vivo* CT imaging effect of Bi_2S_3 nanorods. Before the injection of Bi_2S_3 nanorods, the tumor model mice were scanned by CT as a control. After that, the nanostructure dispersion was injected into the tumor model mice by intratumoral injection. **Figure 5c** reveals the CT coronal view of the mouse tumor site before and after intratumoral injection of Bi_2S_3 nanorods (100 μL, 5 mg mL^{-1}). As shown in the **Figure 5c**, the tumor area showed a clear signal after injection compared with that before injection. The tumor site injected with Bi_2S_3 nanorods also showed a brighter contrast then other soft tissues. Additionally, the average CT value of the tumor area increased from 17 to 125. Therefore, Bi_2S_3 nanorods were expected to be used as diagnostic reagents for CT imaging.

As Bi_2S_3 nanorods had excellent photothermal properties, we believed that these nanorods can be used as photothermal therapeutic agents *in vivo*. We explored the photothermal treatment effect of Bi_2S_3 nanorods on tumor model mice driven by 808 nm laser. EL-4 cell tumor model mice were randomly divided into four groups (see experimental section) and received different treatments. During the 808 nm laser treatment, an infrared camera can be used to obtain an infrared thermal image of the whole body of the mouse. After 100 s, the surface temperature of the Group 4 (injected Bi_2S_3 nanorods and then irradiated with an 808 nm laser at 0.5 W cm^{-2}) increased to ∼55°C, while the temperature change of Group 1 (only 808 nm laser irradiation) didn't not increase significantly as the irradiation time was extended (**Figure 6A**). These results indicated that the Bi_2S_3 nanorods still had a good photothermal effect *in vivo*. After the corresponding treatment, we recorded the change in tumor volume 2 days using vernier calipers. As shown in **Figure 6B**, the tumor disappears without recurrence only for the mice in Group 4. The tumor volume of mice in Group 3was

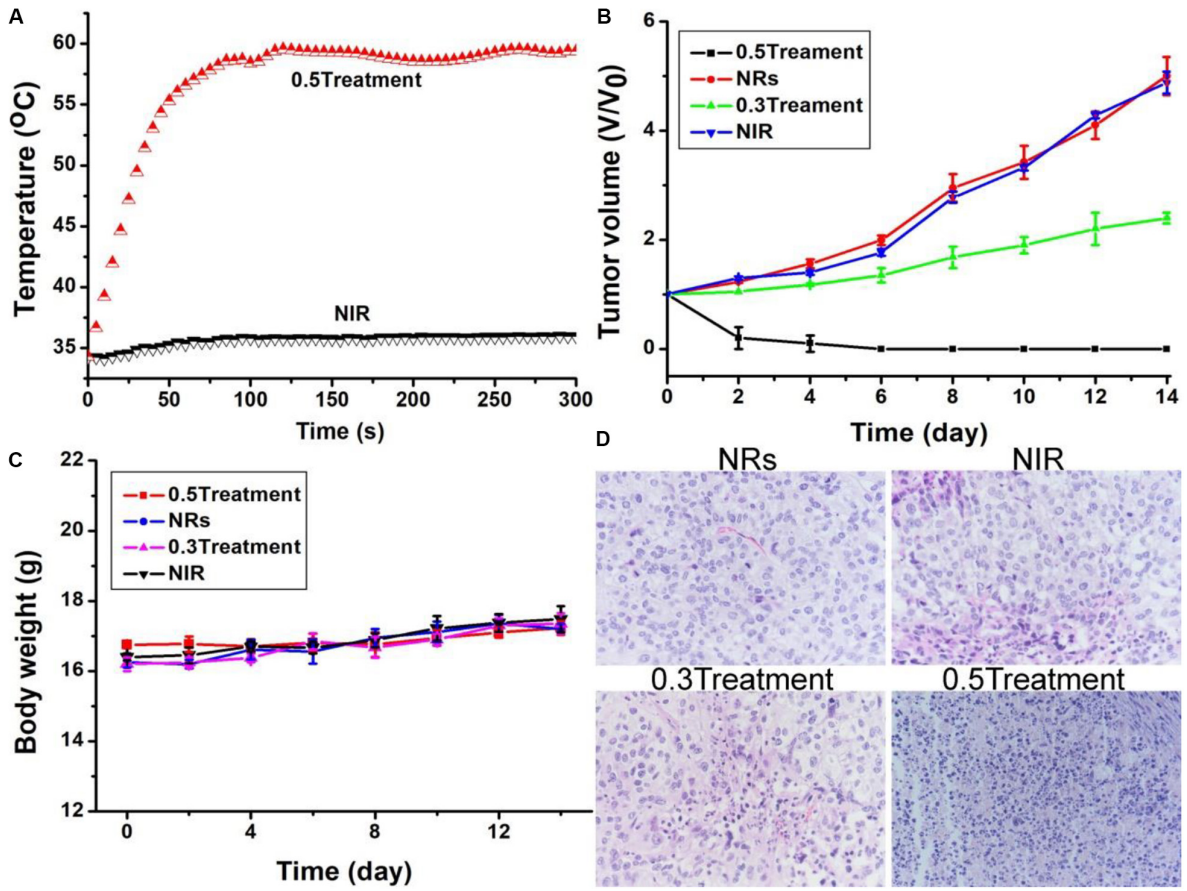

FIGURE 6 | (A) Photothermal effect after injection of PBS, and Bi_2S_3 nanorods under the irradiation of the 808 nm laser with a power density of 0.5 W cm^{-2}, respectively. **(B)** Tumor volume and **(C)** Body weight changes in different groups. **(D)** H&E images of *ex vivo* tumor sections in different groups. Magnification: 200 times.

significantly inhibited but the tumor was still growing because the laser power density in Group 3 was lower. Although the photothermal effect from the nanorods (40 ppm) could efficiently kill cancer cells *in vitro* under the irradiation of the 808 nm laser (0.3 W cm^{-2}), the power density of the lasers will be attenuated when the laser passes through the skin of the mice, making the inhibition of tumor growth rather than complete elimination in Group 3. The tumors of the mice in the other two control groups were not suppressed, and the tumor growth curves between the two groups were almost indistinguishable. We also tested the weight changes of each group of mice after the indicated treatment. There was no significant difference between the four groups of mice (**Figure 6C**), indicating that the treatment conditions we gave showed no side effects.

After treatment, all tumors were taken out and made into 4 μm slices. The slices were stained with H&E. The micrographs after staining are shown in **Figure 6D**. As expected, compared with Group 3 and 4, the changes in size, morphology and cell nuclear were not clearly observed in the Groups 1 and 2 injected with nanorods alone or only irradiated with laser. Cell necrosis in Groups 1 and 2 was only ∼5.3 and 8.7%, respectively (**Supplementary Figure S3**). However, cancer cells injected with nanorods showed severe cell destruction after laser irradiation. After co-treatment with nanorods and lasers, cell necrosis such as nuclear shrinkage, nuclear rupture, and nuclear dissolution occurred. In addition, as the laser power density was increased from 0.3 W cm^{-2} to 0.3 W cm^{-2}, more cell necrosis was observed. It can be observed that the interstitial structure around the cells is more severely damaged, and some cells are completely detached from the cells in Group 4. The tumor cell necrosis rate in Groups 3 and 4 was 55.2 and 90.8%, respectively. These results indicated that cancer cells *in vivo* can be effectively killed by the photothermal effect of Bi_2S_3 nanorods. Therefore, the combination of Bi_2S_3 nanorods and 808 nm laser is very feasible for photothermal therapy of cancer cells.

Photothermal agents should have excellent biocompatibility. We first studied the biodistribution of the Bi_2S_3 nanorods. Healthy mice were intravenously injected with 10 mg·kg^{-1} of the Bi_2S_3 nanorods. Major organs, including lung, liver, spleen, kidney and heart, were achieved at different time points (i.e., 1, 7, 14, 21 days, n = 3). These organs were then solubilized, and determined by ICP-AES analysis to confirm the content of bismuth. It showed (**Supplementary Figure S4**) that the Bi_2S_3 nanorods mainly accumulate in

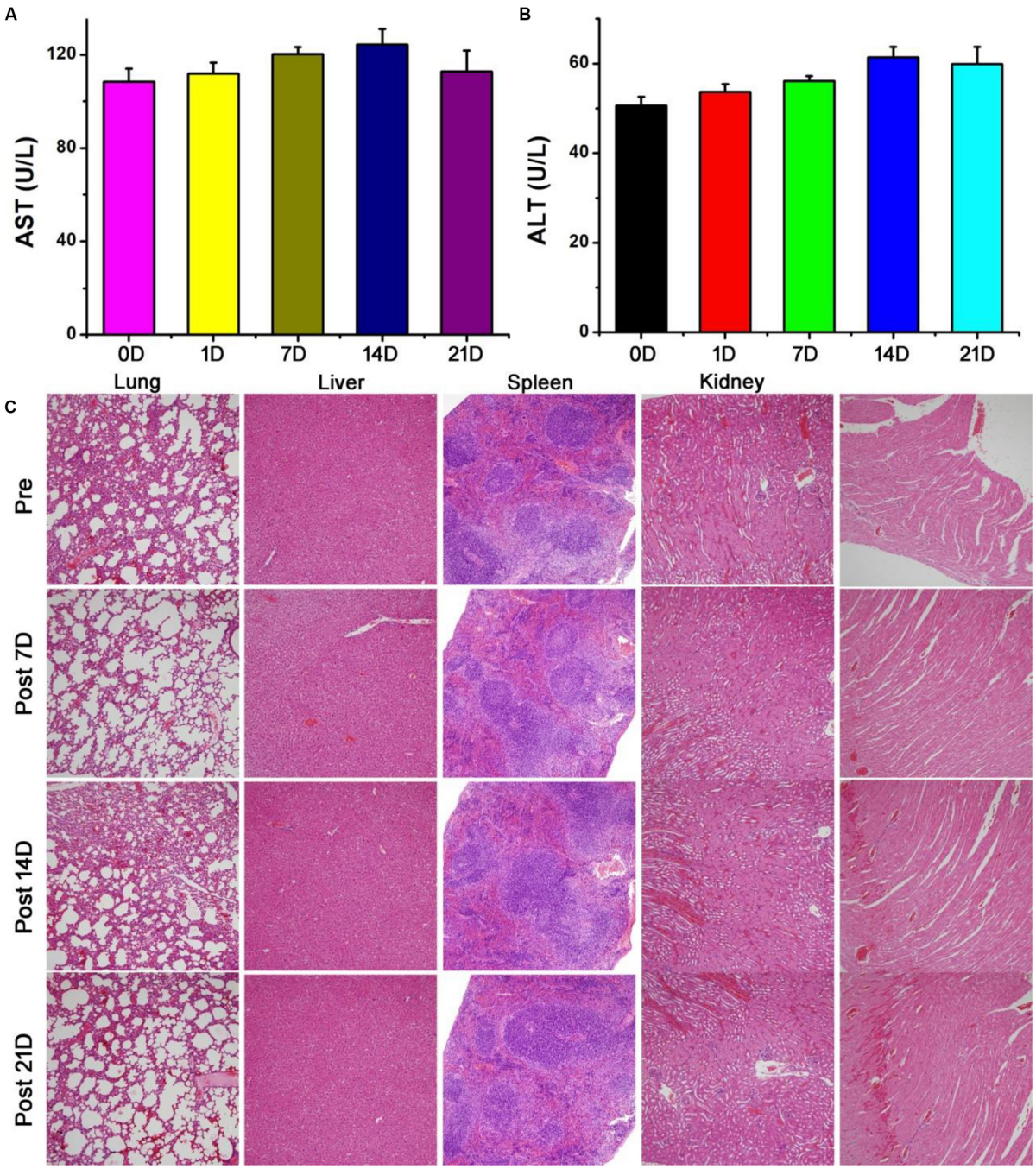

FIGURE 7 | Blood biochemical results of control group and Bi_2S_3 nanorod at different time points (1, 7, 14, 21 days) after injection: **(A)** aspartate aminotransferase (AST), **(B)** alanine aminotransferase (ALT). **(C)** HE analysis of main organs at different time points (0, 7, 14, 21 days) after injection, including lung, liver, spleen, kidney and heart. Magnification: 100 times.

the liver and spleen after the intravenous administration, indicating that Bi_2S_3 nanorods were mainly degraded through these two organs. Furthermore, blood samples from the Bi_2S_3 nanorod group and PBS group were collected at the different time points (i.e., 0, 1, 7, 14, 21 days). No obvious difference was observed in the aspartate aminotransferase (AST, **Figure 7A**) and alanine aminotransferase (ALT, **Figure 7B**), indicating that Bi_2S_3 nanorods showed little influence on liver and kidney at the given dose. In addition, the major organs were collected for histological analysis pre- and post-injection of Bi_2S_3 nanorods at varied time points (i.e., 7, 14, 21 days). No obvious organ damage, such as the change of the

shape and size of the cells, were noted compared with the control group (**Figure 7C**). The results suggested that the Bi_2S_3 nanorods showed good biocompatibility.

CONCLUSION

In conclusion, the Bi_2S_3 nanorods were successfully prepared by a facile solvothermal synthesis method to be served as a promising photothermal theragnosis agent. The Bi_2S_3 nanorods exhibited a strong NIR absorption band due to the special shape and defects, thus showed amazing photothermal effect with a photothermal conversion efficiency as high as 78.1%. The photothermal ablation experiment of cells both *in vitro* and *in vivo* prove that the Bi_2S_3 nanorods have a good photothermal effect under the irradiation of an 808 nm laser and can effectively kill cancer cells. *In vivo* and *in vitro* CT imaging experiments demonstrate that Bi_2S_3 nanorods are expected to be effective CT imaging agents. Therefore, the Bi_2S_3 nanorods can be used as promising photothermal theragnosis agents due to the excellent photothermal effect, CT imaging capability and low toxicity.

DATA AVAILABILITY STATEMENT

All datasets presented in this study are included in the article/**Supplementary Material**.

ETHICS STATEMENT

The animal study was reviewed and approved by Huashan Hospital, Fudan University.

AUTHOR CONTRIBUTIONS

JJ and ZW designed the project. JJ, XC, YQ, and LW carried out the experiment. JJ, YZ, and ZW performed the experimental data analysis. JJ and ZW wrote the manuscript. All authors contributed to discussion of the results.

FUNDING

This study was supported by the National Natural Science Foundation of China (81670868).

SUPPLEMENTARY MATERIAL

The Supplementary Material for this article can be found online at: https://www.frontiersin.org/articles/10.3389/fmats.2020.00234/full#supplementary-material

REFERENCES

Ai, K., Liu, Y., Liu, J., Yuan, Q., He, Y., and Lu, L. (2011). Large-scale synthesis of Bi2S3Nanodots as a contrast agent for in vivo X-ray computed tomography imaging. *Adv. Mater.* 23, 4886–4891. doi: 10.1002/adma.201103289

Chang, J.-Y., Lin, J.-M., Su, L.-F., and Chang, C.-F. (2013). Improved performance of $cuins_2$ quantum dot-sensitized solar cells based on a multilayered architecture. *ACS Appl. Mater. Interf.* 5, 8740–8752.

Chen, H., Shao, L., Ming, T., Sun, Z., Zhao, C., Yang, B., et al. (2010). Understanding the photothermal conversion efficiency of gold nanocrystals. *Small* 6, 2272–2280. doi: 10.1002/smll.201001109

Chen, Z., Wang, Q., Wang, H., Zhang, L., Song, G., Song, L., et al. (2013). Ultrathin PEGylated $W_{18}O_{49}$ nanowires as a new 980 nm-laser-driven photothermal agent for efficient ablation of cancer cells in vivo. *Adv. Mater.* 25, 2095–2100. doi: 10.1002/adma.201204616

Hessel, C. M., Pattani, V. P., Rasch, M., Panthani, M. G., Koo, B., Tunnell, J. W., et al. (2011). Copper selenide nanocrystals for photothermal therapy. *Nano Lett.* 11, 2560–2566. doi: 10.1021/nl201400z

Li, B., Wang, Q., Zou, R., Liu, X., Xu, K., Li, W., et al. (2014). $Cu_{7.2}S_4$ nanocrystals: a novel photothermal agent with a 56.7% photothermal conversion efficiency for photothermal therapy of cancer cells. *Nanoscale* 6, 3274–3282.

Li, B., Ye, K., Zhang, Y., Qin, J., Zou, R., Xu, K., et al. (2015). Photothermal theragnosis synergistic therapy based on bimetal sulphide nanocrystals rather than nanocomposites. *Adv. Mater.* 27, 1339–1345. doi: 10.1002/adma.201404257

Li, J., Jiang, F., Yang, B., Song, X. R., Liu, Y., Yang, H. H., et al. (2013). Topological insulator bismuth selenide as a theranostic platform for simultaneous cancer imaging and therapy. *Sci. Rep.* 3:1998.

Li, J. C., Rao, J. H., and Pu, K. Y. (2018). Recent progress on semiconducting polymer nanoparticles for molecular imaging and cancer phototherapy. *Biomaterials* 155, 217–235. doi: 10.1016/j.biomaterials.2017.11.025

Li, W., Zamani, R., Rivera Gil, P., Pelaz, B., Ibanez, M., Cadavid, D., et al. (2013). CuTe nanocrystals: shape and size control, plasmonic properties, and use as SERS probes and photothermal agents. *J. Am. Chem. Soc.* 135, 7098–7101. doi: 10.1021/ja401428e

Liu, H., Liu, T., Wu, X., Li, L., Tan, L., Chen, D., et al. (2012). Targeting gold nanoshells on silica nanorattles: a drug cocktail to fight breast tumors via a single irradiation with near-infrared laser light. *Adv. Mater.* 24, 755–761. doi: 10.1002/adma.201103343

Liu, J., Yang, Y., Zhu, W., Yi, X., Dong, Z., Xu, X., et al. (2016). Nanoscale metal-organic frameworks for combined photodynamic & radiation therapy in cancer treatment. *Biomaterials* 97, 1–9.

Poper, D. K., Ahn, W., and Hoepfner, M. (2007). Microscale heat transfer transduced by surface plasmon resonant gold nanoparticles. *J. Phys. Chem. C* 111, 3636–3641. doi: 10.1021/jp064341w

Robinson, J. T., Welsher, K., Tabakman, S. M., Sherlock, S. P., Wang, H., Luong, R., et al. (2010). High performance in vivo near-IR (>1 mum) imaging and photothermal cancer therapy with carbon nanotubes. *Nano Res.* 3, 779–793. doi: 10.1007/s12274-010-0045-1

Roper, D. K., Ahn, W., and Hoepfner, M. (2007). Microscale heat transfer transduced by surface plasmon resonant gold nanoparticles. *J. Phys. Chem. C* 111, 3636–3641. doi: 10.1021/jp064341w

Song, G., Liang, C., Gong, H., Li, M., Zheng, X., Cheng, L., et al. (2015). Core-shell MnSe@Bi_2Se_3fabricated via a cation exchange method as novel nanotheranostics for multimodal imaging and synergistic thermoradiotherapy. *Adv. Mater.* 27, 6110–6117. doi: 10.1002/adma.201503006

Tian, Q., Hu, J., Zhu, Y., Zou, R., Chen, Z., Yang, S., et al. (2013). Sub-10 nm Fe_3O_4@$Cu_{2-x}S$ core-shell nanoparticles for dual-modal imaging and photothermal therapy. *J. Am. Chem. Soc.* 135, 8571–8577. doi: 10.1021/ja4013497

Tian, Q., Jiang, F., Zou, R., Liu, Q., Chen, Z., Zhu, M., et al. (2011). Hydrophilic Cu_9S_5 nanocrystals: a photothermal agent with a 25.7% heat conversion efficiency for photothermal ablation of cancer cells in vivo. *ACS Nano* 5, 9761–9771. doi: 10.1021/nn203293t

Wang, C., Chen, J., Talavage, T., and Irudayaraj, J. (2009). Gold nanorod/Fe_3O_4 nanoparticle "nano-pearl-necklaces" for simultaneous targeting, dual-mode

imaging, and photothermal ablation of cancer cells. *Angew. Chem. Int. Ed. Engl.* 48, 2759–2763. doi: 10.1002/anie.200805282

Xie, H., Shao, J., Wang, J., Sun, Z., Yu, X.-F., and Wang, Q.-Q. (2017). Near-infrared optical performances of two Bi_2Se_3 nanosheets. *RSC Adv.* 7, 50234–50238. doi: 10.1039/c7ra09872c

Xu, G., Yamada, T., Otsubo, K., Sakaida, S., and Kitagawa, H. (2012). Facile "modular assembly" for fast construction of a highly oriented crystalline MOF nanofilm. *J. Am. Chem. Soc.* 134, 16524–16527. doi: 10.1021/ja307953m

Yang, G., Phua, S. Z. F., Bindra, A. K., and Zhao, Y. (2019). Degradability and clearance of inorganic nanoparticles for biomedical applications. *Adv. Mater.* 31:e1805730.

Zhang, S., Sun, C., Zeng, J., Sun, Q., Wang, G., Wang, Y., et al. (2016). Ultrasmall PEGylated $Cu_{2-x}Se$ nanoparticles as a multifunctional theranostic agent for multimodal imaging guided photothermal therapy of cancer. *Adv. Mater.* 28, 8927–8936. doi: 10.1002/adma.201602193

Conflict of Interest: The authors declare that the research was conducted in the absence of any commercial or financial relationships that could be construed as a potential conflict of interest.